REGULAR ARTICLE

Effects of functional group position on hole transporting properties of carbazole derivatives in perovskite solar cells

Jianyu Cui, Wei Rao, Rongxing He*

¹Key Laboratory of Luminescence and Real-Time Analytical Chemistry (Southwest University), Ministry of Education, College of Chemistry and Chemical Engineering, Southwest University, Chongqing 400715, China

Received 12 Nov. 2017; Accepted (in revised version) 25 Dec. 2017

Abstract: Several carbazole derivatives (V866, V867 and V868) as hole transporting materials (HTMs) in perovskite solar cells are designed to explore the functional group position effect on electrochemical properties. The material properties are studied on the first-principle calculations combined with the Marcus theory. The results illustrate that V866 (*ortho*-position) has the suitable HOMO energy level matched with the metal electrode (-5.1 eV) and the perovskite absorption layer (-5.4 eV). Moreover, the molecular planarity of HTMs with the *ortho*-position functional groups is improved, which enhances intermolecular face-to-face π - π stacking degree. Compared to V867 and V868, the largest hole mobility value (0.007 cm² V⁻¹ s⁻¹) of V866 is obtained due to its modified molecular planarity. Therefore, V866 (*ortho*-position) is indeed an excellent carbazole HTM. Our theoretical investigation of HTMs is helpful for understanding the hole transporting behaviors and developing higher performance HTMs.

Keyword: HTM; Carbazole derivatives; Hole mobility; PSC; Molecular planarity

1. Introduction

Hybrid lead halide perovskite solar cells (PSCs) have attracted wide interest in recent years,

^{*} Corresponding author. *E-mail address:* herx@swu.edu.cn

due to their high power conversion efficiency (PCE), facile processability, relatively cheap raw material and manufacturing cost [1-5]. Lately, it is reported that the highest PCE has reached 22%. The rapid development of PSCs attributes to the simultaneous development of device assembly technology, excellent perovskite absorption layers and suitable charge transporting layers. In the charge transporting layers, the hole transport layer is introduced to construct Ohmic contact and eliminate the Schottky contact between the perovskite absorbing layer and the metal electrode [6]. The construction of ohmic contact is an important way to improve charge transfer ability. Therefore, the hole transporting layer has been extensively explored due to its important role in PSCs.

As far as we know, most of PSCs have been assembled with spiro-OMeTAD as HTMs [7-14]. The PCE of the solar cells assembled with spiro-OMeTAD as HTMs has risen rapidly from 9.4% to 22% in recent years [15-18]. However, the synthesis of Spiro-OMeTAD is excessively expensive due to its complex synthesis steps and harsh synthesis conditions [19]. Thus, tremendous effort has been spared on synthesizing alternative molecules by many research groups [20-22]. However, the achieved PCE of PSCs using non spiral ring molecules as HTMs is very low. Most of these molecules fail to show performance similar to that of Spiro-OMeTAD. The only HTM without the spiro motif, known to date that demonstrated device efficiency close to 15% requires custom-made boronic acids as precursors for the final synthesis.

Recently, Gratia reported a new type of hole transporting twin molecule V866, based on methoxydiphenylamine-substituted carbarzole, with performance very similar to that of Spiro-OMeTAD [19]. The PSCs employing V886 as HTMs show the PCE up to 16.91%. Moreover, V866 does not require an extensive and expensive synthetic procedure. This is the highest PCE that can be achieved by using non spiral ring dopant-free molecules as HTMs at present. Furthermore, its simple two-step synthesisthe ready availability of the starting materials makes V866 very appeale for commercial prospects of PSCs [19]. Therefore, we choose V866 as our investigated subject.

Although the HTMs in PSCs have been extensively studied in experiment, few researchers have systematically studied the electrochemical properties of hole transporting materials in theory. Therefore, we plan to study the hole transporting properties based on the first-principle calculations combined with the Marcus theory [23]. Several experimental paper has pointed out that the introduction of a conjugated core into HTMs in PSCs can enhance the intermolecular hole mobility [15, 24]. However, little attention has been paid to the effect of the functional groups on the conjugated core, such as the benzene ring in HTMs. Based on this idea, V866 (*ortho*-position), V867 (*meta*-position) and V868 (*para*-position) are developed to study the effect on anisotropic hole mobility when the functional groups position changes in HTMs. Here, the functional group is methoxydiphenylamine-substituted

carbazole group (MSCG). The results show that the suitable HOMO level of V866 allows it to have enough hole injection driving force from the perovskite absorbing layer to the metal electrode when the MSCG is in the *ortho*-position,. Furthermore, compared with V867 (*meta*-position) and V868 (*para*-position), the hole mobility ability of V866 (*ortho*-position) is also effectively enhanced due to the improved molecular plarity. Therefore, V866 is indeed a primarizing HTM with excellent electrochemical properties. Our work may provide a theoretical exploration for designing high-performance HTMs.

2. Computational methods

In this work, the hole transporting properties of all invested molecules are based on a combination of first-principles quantum mechanic calculations and Marcus theory. The hopping mechanism is used to describe the hole transfer and the transfer rate (*W*) for all investigated molecules is expressed as [25, 26]:

$$W = \frac{V^2}{\hbar} \left(\frac{\pi}{\lambda k_B T} \right)^{1/2} \exp\left(-\frac{\lambda}{4k_B T} \right), \tag{1}$$

Herein, V denotes the intermolecular electronic coupling of a dimer [27]. k_B represents the Boltzmann constant, T is the temperature in Kelvin and h denotes the Planck constant. λ represents reorganization energy, which is calculated by using the adiabatic potential energy surface method [28, 29]. λ can be expressed in Eq. (2).

$$\lambda = (E_0^* - E_0) + (E_+^* - E_+), \tag{2}$$

 E_0^* and E_+^* denote the energies of the neutral and cationic states with the geometries of the cationic and neutral species. E_0 and E_+ are the energies of the neutral and cationic species in their lowest-energy geometries [23].

$$V = \frac{J_{RP} - S_{RP} \left(H_{RR} + H_{PP} \right) / 2}{1 - S_{PP}^2},$$
(3)

Where H_{RR} and H_{PP} represent the site energies. S_{RP} is the spatial overlap and J_{RP} is the charge transfer integrals for one dimer.

Hole mobility is used to evaluate hole transporting process, which is expressed as follows [23]:

$$\mu_{\Phi} = \frac{e}{2k_B T} \sum_{i} W_i r_i^2 P_i \cos^2 \gamma_i \cos^2 \left(\theta_i - \Phi\right), \tag{4}$$

 γ_i denotes the dihedral angle between the hole transporting pathways and the chosen crystal plane [30]. In general, the plane where all the transmission paths lie is parallel to the chosen crystal plane, and at this point γ_i is 0. Φ denotes the orientation angle between the hole transporting channel and the chosen crystal axis [31]. This orientation angle is the

vector synthesis result of the hole mobility of all hole hopping paths [32]. θ represent the angle between the hole hopping pathway and the chosen crystal axis. r_i is the intermolecular centroid distance of the dimer. Herein, for a dimer, θ and r_i is directly measured by Materials Studio software (MS) [33-38]. P_i denotes the hopping probability of a pathway, which could be calculated by Eq. (5). W_i denotes the transfer rate of one dimer.

$$P_{i} = \frac{W_{i}}{\sum_{i} W_{i}}, \tag{5}$$

All the optimization of molecular structure are performed by Gaussian09 software package on the basis of the density functional theory (DFT) [39]. A series of functionals are tested for choosing suitable HOMO energy levels coinciding with experiment values [40, 41]. According to the comparison of different methods, only the HOMO energy levels (-5.326 eV) calculated by hybrid functional B3P86/6-311G(d) is the closest to the experimental value (-5.27 eV). Therefore, the hybrid functional B3P86/6-311G(d) applies to our research system. Due to the solvent effect, the polarized continuum model (PCM) equilibrium solvation is adopted in the ground state optimization. The required parameters (H_{RR} , H_{PP} S_{RP} and J_{RP}) to calculate electronic coupling (V) for different dimers are implemented in Amsterdam density functional (ADF) program [42]. Here, the local density functional VWN in the conjunction with the PW91 gradient corrections with the TZ2P basis set in the energy calculation is chosen for all the invested molecules. Herein, the crystal data is predicted by Materials Studio software (MS) [43] based on common space groups $P_{21/c}$, P_{-1} , $P_{21}2_{12}1$, P_{21} , $C_{2/c}$, P_{bca} , $P_{na}2_1$, P_{bcn} , C_2 and C_c in Dreiding forcefield [44]. These space groups characterize most of all molecular crystals consisting of organic compounds [45, 46].

3. Results and discussion

All the geometries of material molecules investigated here are illustrated in **Figure 1**. As shown in **Table 1**, the HOMO energy levels of V866, V867 and V868 are -5.326 eV, -4.720 eV and 4.697 eV, respectively. In PSCs, the HOMO energy level is an important parameter to evaluate the hole injection driving forces. Generally, the HOMO energy levels of the perovskite absorbing layer and metal electrode are -5.4 eV and -5.1 eV from the schematic of PSC [47]. Although the higher HOMO energy level enables the material molecules to obtain stronger hole injection driving forces from the perovskite absorption layer to the hole transporting layer, it is not conducive to hole transfer process from hole transporting layer to the metal electrode. Therefore, only the HOMO energy level of V866 matches the perovskite absorption layer and the metal electrode perfectly. Furthermore, in order to hinder the electron transportation from perovskite absorbing layer to the metal electrodes, the LUMO energy level should be higher than the conduction band level of perovskite absorbing layer

such as CH₃NH₃PbI₃ (-3.93 eV). The LUMO energy level of V866, V867 and V868 is -1.970 eV, -1.283 eV and -1.267 eV, respectively. Therefore, the LUMO energy levels of these three molecules are much higher than the conduction band level of the perovskite absorption layer, which can hinder the backflow of electrons effectively.

The optical bandgap (Eg) is the energy difference value between HOMO and LUMO energy levels. Some papers point out that smaller bandgap of a semiconductor is conductive to increase the intrinsic electrical conductivity by increasing the carrier concentration [48-51]. Eg values of V866, V867 and V868 is 3.390 eV, 3.437 eV and 3.430 eV, respectively. Therefore, the intrinsic electrical conductivity of V866 is larger than that of V867 and V868. The orbital spatial distribution and components of the HOMO and LUMO for these molecules are described in **Figure 2**. For these three molecules, the HOMO orbitals are almost populated over the benzene connected with methoxy and the carbazole. The LUMO orbitals are almost centered on the carbazole. However, the orbital overlap between the HOMOs and LUMOs remains slightly different. For V867 and V868, the orbital overlap between the HOMOs and LUMOs is larger than that of V866. The larger orbital overlap between the HOMOs and LUMOs suggests that fast formation of neutral excitons and hole may take place [52]. It can be seen that the hole transporting performance of V866 may be better than the performances of V867 and V868.

Figure 1: Molecular structures of V866, V867 and V868.

From **Table 1**, the reorganization energy of V866 is the smallest. The reorganization energy of V868 is slightly smaller than that of V867. According to Eq. (1), larger reorganization energy is not helpful for higher transfer rate *W*. Thus, V866 may possess higher transfer rate than V867 and V868.

As shown in **Figure 3**, the dihedral angle of two carbazole ring planes for V866, V867 and V868 is 7.29°, 60.2° and 10.31°, respectively. The dihedral angle for V866 is smaller than the other dihedral angles for V867 and V868. Herein, material molecules with smaller dihedral angle of two carbazole ring planes possess better molecular planarity. Good molecular planarity is beneficial to the formation of intermolecular face-to-face π - π stacking increasing the hole mobility between conjugated molecules. Therefore, compared with V867 and V868, V866 may have the largest hole mobility.

Table 1. HOMO and LUMO energy level, the optical bandgap (E_g) and the reorganization energy (λ) of all the molecules at level of B3P86/6-311G(d).

Molecules	HOMO (eV)	LUMO (eV)	Eg (eV)	λ (eV)
V866	-5.326	-1.936	3.390	9.897×10 ⁻²
V867	-4.720	-1.283	3.437	1.262×10 ⁻¹
V868	-4.697	-1.267	3.430	1.069×10 ⁻¹

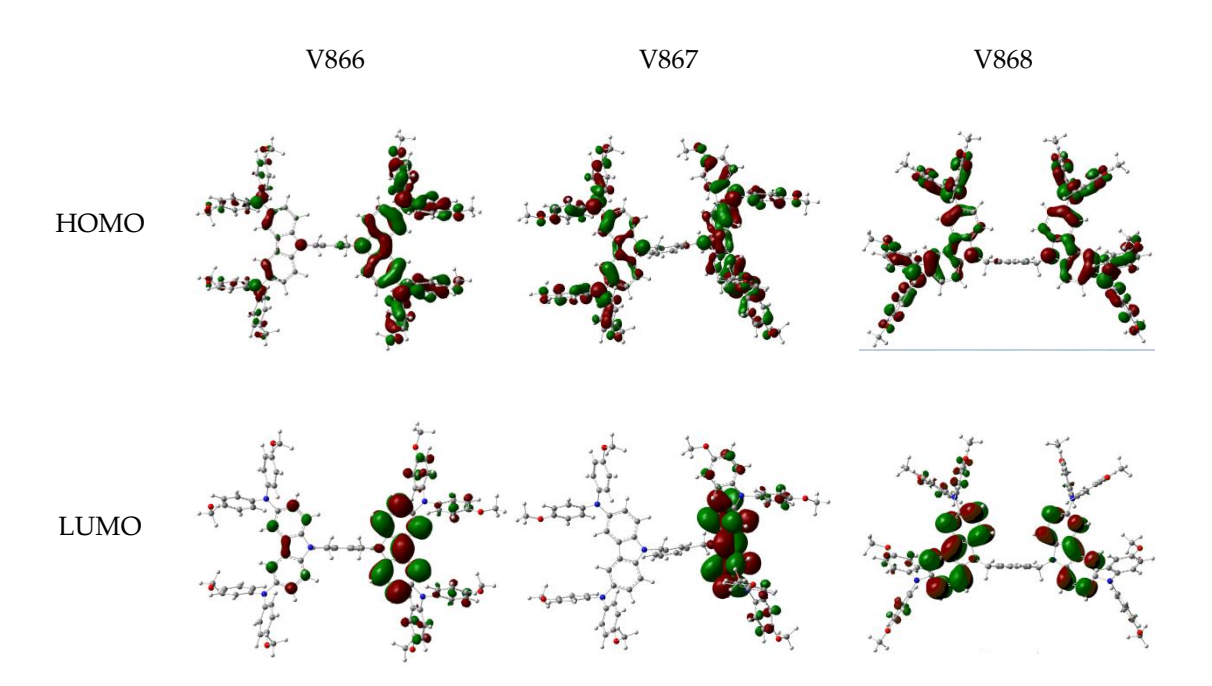


Figure 2: Frontier molecular orbitals of all the molecules at level of B3P86/6-311G(d).

Herein a first-principles-based simulation is used to predict intrinsic carrier transport behavior of organic crystals with crystal structures [23]. We cannot find the crystal structure data of V866, V867 and V868 in all databases. Thus, the crystal structures of invested molecules are predicted based on different space groups. Energy data from different crystal data are listed in **Figure 4**. It shown that three molecules have their respective lowest points in energy when the horizontal coordinate is *P21*. The crystal structure with the lowest energy is the most stable. The lattice parameters of three crystal structures are listed in **Table 2**.

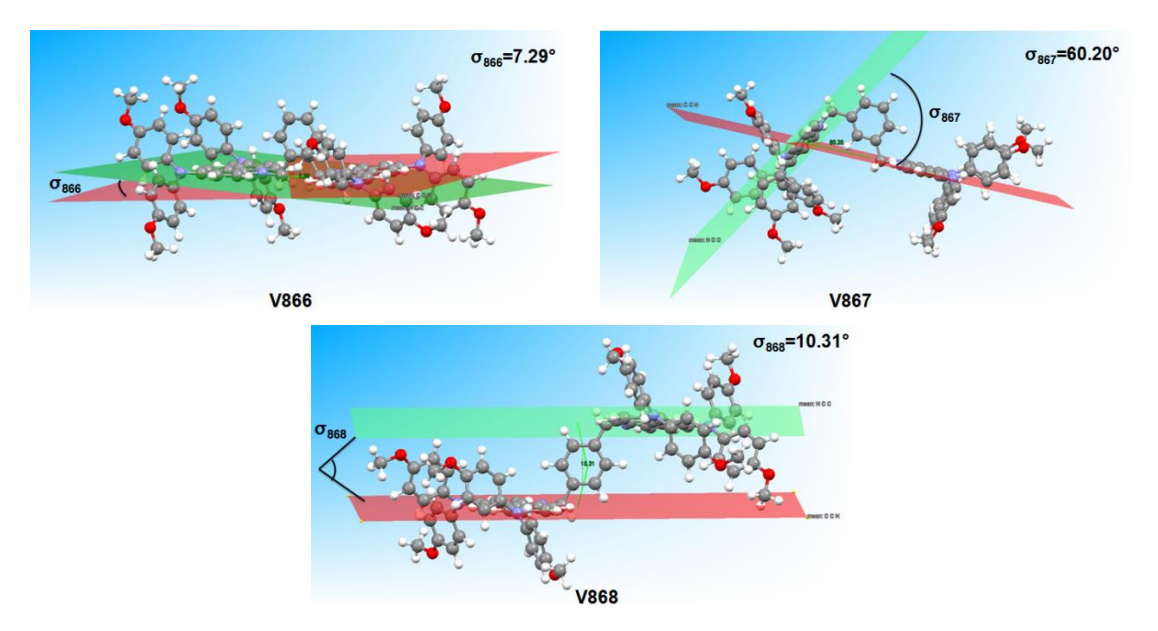


Figure 3: The dihedral angles of two carbazole ring planes for V866, V867 and V868.

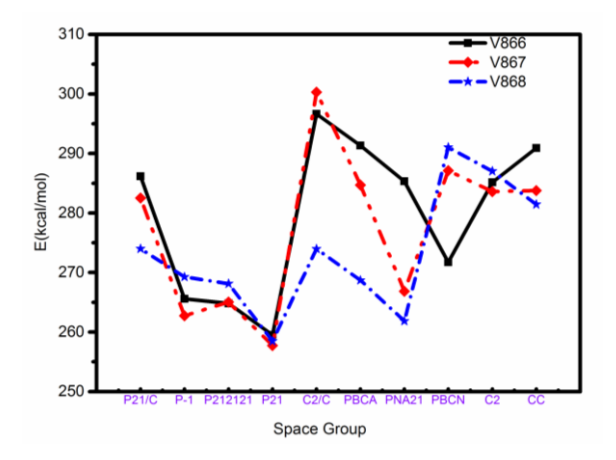


Figure 4: The energy distribution of crystal structures on different space groups for V866, V867 and V868.

All the dimers are characterized as transverse (T) dimer, parallel (P) dimer. For these three molecules, different dimers are found on crystal surface bc as shown in **Figure 5**. For V866, the centroid distance r of T1 dimer is equal to of the intermolecular centroid distance r of T3 dimer. However, the electronic coupling value V of T1 dimer is larger than that of T3 dimer. Thus, the centroid distance r may not be the only determinant of the electron coupling and hole mobilty. The electronic coupling value V of T1 dimer for V867 and V868 is 0 eV. The intermolecular centroid distance r is so far away that the electronic coupling effect is very small. For V866, V867 and V868, the maximum values of electron coupling are -1.452×10^{-3} eV, 7.281×10^{-4} eV and -1.052×10^{-3} eV, resipectively. Futhermore, at this time, the intermolecular centroid distances for V866, V867 and V868 are for 12.3 Å, 12.0 Å and 10.2 Å, respectively. Therefore, compared with V867 and V868, the strongest electron coupling effect of V866 is obtained due to the best molecular planarity.

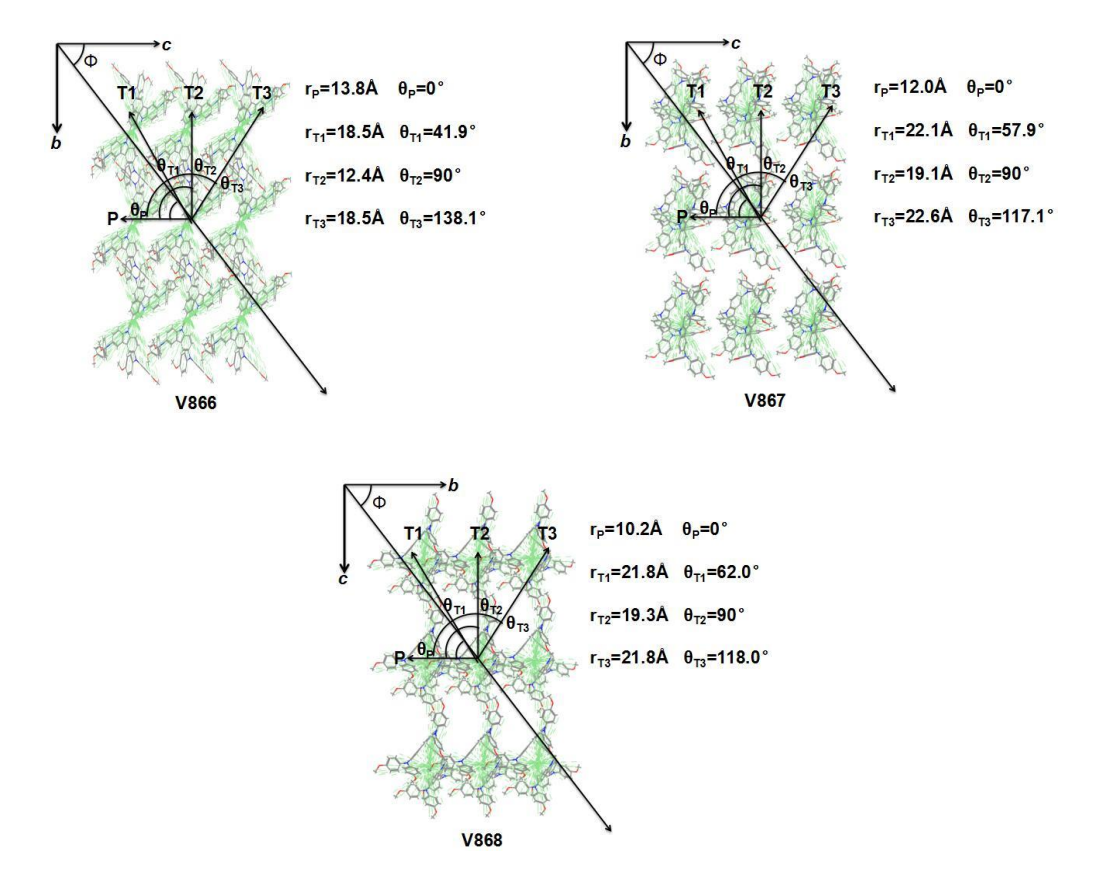


Figure 5: Comparison of molecular packings and charge hopping pathways in V866 (bc), V867 (bc) and V868 (bc) with the centroid distance r (Å) and the angle of the projected electronic coupling pathways relative to the reference axis. The long black arrow represents the transport channel.

From **Table 3**, it shows that the μ_{max} of V866, V867 and V868 are 0.007 cm² V⁻¹ s⁻¹, 0.002 cm² V⁻¹ s⁻¹ and 0.003 cm² V⁻¹ s⁻¹. Good molecular planarity is favorable for generating the face-to-face π - π packing. The face-to-face π - π packing with larger orbital overlap could contribute to stronger electronic coupling effect. Thus, the highest hole mobility of V866 (*ortho*-position) is obtained due to the face-to-face π - π packing. In conclusion, V866 is a promising hole transporting material indeed.

All the calculated hole mobility μ for V866, V867 and V868 are given in **Figure 6**. Understanding the anisotropic hole mobility can be helpful to control the orientation of charge transport channel relative to the reference axis of molecular crystal [32]. Angular-resolution anisotropic mobility curve of V866 is different from the curves of V867 and V868. The reason is that the hole mobility of P dimer is closed to the hole mobility of T2 dimer for V866. Here we choose the crystal axis c as the reference axis for V866. There is maximum hole mobility value (0.007 cm² V⁻¹ s⁻¹) along to the crystal axis b direction for V866 when Φ angle is 0°/180°. However, the maximum hole mobility value along to the crystal axis b direction for V867 and V868 are near 90°/270° in the angle-resolution figure, which are 0.002 cm² V⁻¹ s⁻¹ and 0.003 cm² V⁻¹ s⁻¹, respectively.

Table 2. The lattice parameters of the crystal structures for V866, V867 and V868.

Molecules	Lattice parameters (Å)				
V866	cubic27.790×12.359×13.762 Å ³	α=90.000°, β=63.983°, γ=90.000°			
V867	cubic19.745×11.994×19.098 Å ³	α =90.000°, β =100.804°, γ =90.000°			
V868	cubic23.389×10.247×19.295 Å ³	α =90.000°, β =104.616°, γ =90.000°			

Table 3. The intermolecular centroid distance r (Å), the electronic coupling value V(eV) and the μ_{max} (cm² V⁻¹ s⁻¹) for V866, V867 and V868.

pathway –	V866		V86	V867		V868	
	V	r	V	r	V	r	
P	-1.311×10 ⁻³	13.8	7.281×10 ⁻⁴	12.0	-1.052×10 ⁻³	10.2	
T1	3.903×10 ⁻⁵	18.5	0	22.6	0	21.8	
T2	-1.452×10 ⁻³	12.3	8.604×10 ⁻⁵	19.1	4.271×10 ⁻⁴	19.3	
Т3	-1.057×10 ⁻⁵	18.5	1.000×10 ⁻⁵	22.6	0	21.8	
μ max	0.007		0.00	0.002		0.003	

Compared with V867 (*meta*-position) and V868 (*para*-position), V866 (*ortho*-position) exhibits higher hole mobility in terms of anisotropy. The direction of the charge transporting channel is easy to be controlled so as to obtain a higher hole mobility. It is indicated that the charge transporting properties of V866 are better than that of V867 and V868. It also shows that the functional group position has a great influence on the intermolecular charge-transport properties. The difference can be derived from the relative magnitude of electronic coupling value. It also indicates that free charge in V866 crystal are much more intrinsically mobile than the charge in V867 and V868 crystal. The distribution of angular-resolution anisotropic mobility can help us understand the charge transporting property and design high-performance HTMs.

4. Conclusions

In conclusion, we have developed a series of carbazole derivatives (V866, V867 and V868) as HTMs to explore the functional group position effect on the electrochemical properties. The results illustrate that V866 (ortho-position) has the suitable HOMO energy level matched with the metal electrode and the perovskite absorption layer. Futhermore, compared with V867 (meta-position) and V868 (para-position), a higher hole mobility of V866 (ortho-position) is obtained due to the face-to-face π - π packing. We also find that the functional group position of material molecule plays an important role in determining the molecular stacking configurations and the Angular-resolution anisotropic hole mobility indeed. Our theoretical investigation of carbazole derivatives as HTMs in PSCs may be helpful for evaluating the charge transporting behaviors to realize better charge transfer efficiency and design higher performance HTMs.

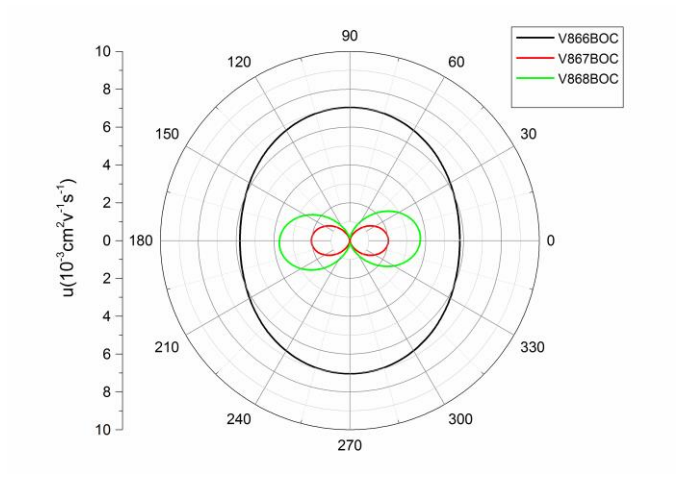


Figure 6: Angular-resolution anisotropic hole mobility curves of V866, V867 and V868.

Acknowledgements

This work was supported by Chongqing Municipal Natural Science Foundation (cstc2013jcyjA90015) and the Fundamental Research Funds for the Central Universities (No. XDJK2013A008).

References

- [1] Z.a. Li, Z. Zhu, C.-C. Chueh, S.B. Jo, J. Luo, S.-H. Jang, A.K.-Y. Jen, Rational Design of Dipolar Chromophore as an Efficient Dopant-Free Hole-Transporting Material for Perovskite Solar Cells, Journal of the American Chemical Society, 138 (2016) 11833-11839.
- [2] M.A. Green, A. Ho-Baillie, H.J. Snaith, The emergence of perovskite solar cells, Nature Photonics, 8 (2014) 506-514.
- [3] S.T. Williams, A. Rajagopal, C.-C. Chueh, A.K.Y. Jen, Current Challenges and Prospective Research for Upscaling Hybrid Perovskite Photovoltaics, The Journal of Physical Chemistry Letters, 7 (2016) 811-819.
- [4] L. Meng, J. You, T.-F. Guo, Y. Yang, Recent advances in the inverted planar structure of perovskite solar cells, Accounts of chemical research, 49 (2015) 155-165.
- [5] P. Docampo, T. Bein, A Long-Term View on Perovskite Optoelectronics, Accounts of Chemical Research, 49 (2016) 339-346.
- [6] Y. Xu, J. Shi, S. Lv, L. Zhu, J. Dong, H. Wu, Y. Xiao, Y. Luo, S. Wang, D. Li, X. Li, Q. Meng, Simple Way to Engineer Metal–Semiconductor Interface for Enhanced Performance of Perovskite Organic Lead Iodide Solar Cells, ACS Applied Materials & Interfaces, 6 (2014) 5651-5656.
- [7] J. Seo, J.H. Noh, S.I. Seok, Rational Strategies for Efficient Perovskite Solar Cells, Accounts of chemical research, 49 (2016) 562-572.
- [8] C.-C. Chueh, C.-Z. Li, A.K.-Y. Jen, Recent progress and perspective in solution-processed Interfacial materials for efficient and stable polymer and organometal perovskite solar cells, Energy & Environmental Science, 8 (2015) 1160-1189.
- [9] Z. Yu, L. Sun, Recent Progress on Hole-Transporting Materials for Emerging Organometal Halide Perovskite Solar Cells, Advanced Energy Materials, 5 (2015).
- [10] S. Ameen, M.A. Rub, S.A. Kosa, K.A. Alamry, M.S. Akhtar, H.S. Shin, H.K. Seo, A.M. Asiri, M.K. Nazeeruddin, Perovskite solar cells: Influence of hole transporting materials on power conversion efficiency, ChemSusChem, 9 (2016) 10-27.
- [11] H. Kim, K.-G. Lim, T.-W. Lee, Planar heterojunction organometal halide perovskite solar cells: Roles of interfacial layers, Energy & Environmental Science, 9 (2016) 12-30.
- [12] M. Liu, M.B. Johnston, H.J. Snaith, Efficient planar heterojunction perovskite solar cells by vapour deposition, Nature, 501 (2013) 395-398.
- [13] N.J. Jeon, H.G. Lee, Y.C. Kim, J. Seo, J.H. Noh, J. Lee, S.I. Seok, o-Methoxy substituents in

- spiro-OMeTAD for efficient inorganic–organic hybrid perovskite solar cells, Journal of the American Chemical Society, 136 (2014) 7837-7840.
- [14] W.S. Yang, J.H. Noh, N.J. Jeon, Y.C. Kim, S. Ryu, J. Seo, S.I. Seok, High-performance photovoltaic perovskite layers fabricated through intramolecular exchange, Science, 348 (2015) 1234-1237.
- [15] K. Rakstys, M. Saliba, P. Gao, P. Gratia, E. Kamarauskas, S. Paek, V. Jankauskas, M.K. Nazeeruddin, Highly Efficient Perovskite Solar Cells Employing an Easily Attainable Bifluorenylidene-Based Hole-Transporting Material, Angewandte Chemie International Edition, 55 (2016) 7464-7468.
- [16] M. Daskeviciene, S. Paek, Z. Wang, T. Malinauskas, G. Jokubauskaite, K. Rakstys, K.T. Cho, A. Magomedov, V. Jankauskas, S. Ahmad, Carbazole-based Enamine: Low-cost and Efficient Hole Transporting Material for Perovskite Solar Cells, Nano Energy, (2017).
- [17] D. Bi, W. Tress, M.I. Dar, P. Gao, J. Luo, C. Renevier, K. Schenk, A. Abate, F. Giordano, J.-P. Correa Baena, J.-D. Decoppet, S.M. Zakeeruddin, M.K. Nazeeruddin, M. Grätzel, A. Hagfeldt, Efficient luminescent solar cells based on tailored mixed-cation perovskites, Science Advances, 2 (2016).
- [18] K.T. Cho, S. Paek, G. Grancini, C.R. Carmona, P. Gao, Y.H. Lee, M.K. Nazeeruddin, Highly efficient perovskite solar cells with a compositional engineered perovskite/hole transporting material interface, Energy & Environmental Science, (2017).
- [19] P. Gratia, A. Magomedov, T. Malinauskas, M. Daskeviciene, A. Abate, S. Ahmad, M. Grätzel, V. Getautis, M.K. Nazeeruddin, A Methoxydiphenylamine-Substituted Carbazole Twin Derivative: An Efficient Hole-Transporting Material for Perovskite Solar Cells, Angewandte Chemie International Edition, 54 (2015) 11409-11413.
- [20] N.J. Jeon, J. Lee, J.H. Noh, M.K. Nazeeruddin, M. Gratzel, S.I. Seok, Efficient inorganic-organic hybrid perovskite solar cells based on pyrene arylamine derivatives as hole-transporting materials, Journal of the American Chemical Society, 135 (2013) 19087-19090.
- [21] P. Qin, S. Paek, M.I. Dar, N. Pellet, J. Ko, M. Gratzel, M.K. Nazeeruddin, Perovskite solar cells with 12.8% efficiency by using conjugated quinolizino acridine based hole transporting material, Journal of the American Chemical Society, 136 (2014) 8516-8519.
- [22] H. Li, K. Fu, A. Hagfeldt, M. Grätzel, S.G. Mhaisalkar, A.C. Grimsdale, A Simple 3, 4-Ethylenedioxythiophene Based Hole-Transporting Material for Perovskite Solar Cells, Angewandte Chemie International Edition, 53 (2014) 4085-4088.
- [23] W.-Q. Deng, L. Sun, J.-D. Huang, S. Chai, S.-H. Wen, K.-L. Han, Quantitative prediction of charge mobilities of π -stacked systems by first-principles simulation, Nature protocols, 10 (2015) 632-642.
- [24] T. Malinauskas, M. Saliba, T. Matsui, M. Daskeviciene, S. Urnikaite, P. Gratia, R. Send, H. Wonneberger, I. Bruder, M. Graetzel, Branched methoxydiphenylamine-substituted fluorene derivatives as hole transporting materials for high-performance perovskite solar cells, Energy & Environmental Science, 9 (2016) 1681-1686.
- [25] R.A. Marcus, J. Chem. Phys., 24 (1956) 966.
- [26] N. Hush, Adiabatic Rate Processes at Electrodes. I. Energy-Charge Relationships, The Journal of

- Chemical Physics, 28 (1958) 962-972.
- [27] K. Senthilkumar, F. Grozema, F. Bickelhaupt, L. Siebbeles, Charge transport in columnar stacked triphenylenes: Effects of conformational fluctuations on charge transfer integrals and site energies, The Journal of chemical physics, 119 (2003) 9809-9817.
- [28] J. Kwiatkowski, J. Nelson, H. Li, J. Bredas, W. Wenzel, C. Lennartz, Simulating charge transport in tris (8-hydroxyquinoline) aluminium (Alq 3), Physical Chemistry Chemical Physics, 10 (2008) 1852-1858.
- [29] T. Yamada, T. Sato, K. Tanaka, H. Kaji, Percolation paths for charge transports in N, N'-diphenyl-N, N'-di (m-tolyl) benzidine (TPD), Organic Electronics, 11 (2010) 255-265.
- [30] X.-Y. Zhang, G.-J. Zhao, Anisotropic charge transport in bisindenoanthrazoline-based n-type organic semiconductors, The Journal of Physical Chemistry C, 116 (2012) 13858-13864.
- [31] S.-H. Wen, A. Li, J. Song, W.-Q. Deng, K.-L. Han, W.A. Goddard III, First-principles investigation of anistropic hole mobilities in organic semiconductors, The Journal of Physical Chemistry B, 113 (2009) 8813-8819.
- [32] S.-H. Wen, A. Li, J. Song, W.-Q. Deng, K.-L. Han, W.A. Goddard, First-Principles Investigation of Anistropic Hole Mobilities in Organic Semiconductors, The Journal of Physical Chemistry B, 113 (2009) 8813-8819.
- [33] J.-L. Brédas, J.E. Norton, J. Cornil, V. Coropceanu, Molecular understanding of organic solar cells: the challenges, Accounts of chemical research, 42 (2009) 1691-1699.
- [34] H. Geng, Q. Peng, L. Wang, H. Li, Y. Liao, Z. Ma, Z. Shuai, Toward quantitative prediction of charge mobility in organic semiconductors: tunneling enabled hopping model, Advanced Materials, 24 (2012) 3568-3572.
- [35] S.M. Ryno, C. Risko, J.-L. Brédas, Impact of molecular packing on electronic polarization in organic crystals: the case of pentacene vs TIPS-pentacene, Journal of the American Chemical Society, 136 (2014) 6421-6427.
- [36] Z. Shuai, H. Geng, W. Xu, Y. Liao, J.-M. André, From charge transport parameters to charge mobility in organic semiconductors through multiscale simulation, Chemical Society Reviews, 43 (2014) 2662-2679.
- [37] Z. Shuai, L. Wang, Q. Li, Evaluation of Charge Mobility in Organic Materials: From Localized to Delocalized Descriptions at a First-Principles Level, Advanced Materials, 23 (2011) 1145-1153.
- [38] L. Wang, G. Nan, X. Yang, Q. Peng, Q. Li, Z. Shuai, Computational methods for design of organic materials with high charge mobility, Chemical Society Reviews, 39 (2010) 423-434.
- [39] M. Frisch, G. Trucks, H. Schlegel, G. Scuseria, M. Robb, J. Cheeseman, G. Scalmani, V. Barone, B. Mennucci, G. Petersson, Gaussian 09, revision D. 01, Gaussian, Inc., Wallingford CT, 2009.
- [40] F. Zhang, P. Yu, W. Shen, M. Li, R. He, Effect of "push-pull" sensitizers with modified conjugation bridges on the performance of p-type dye-sensitized solar cells, RSC Advances, 5 (2015) 64378-64386.
- [41] F. Zhang, P. Yu, Y. Xu, W. Shen, M. Li, R. He, Theoretical investigation of regeneration mechanism of

- the metal-free sensitizer in dye sensitized solar cells, Dyes and Pigments, 124 (2016) 156-164.
- [42] G.t. te Velde, F.M. Bickelhaupt, E.J. Baerends, C. Fonseca Guerra, S.J. van Gisbergen, J.G. Snijders, T. Ziegler, Chemistry with ADF, Journal of Computational Chemistry, 22 (2001) 931-967.
- [43] A.D. Studio, 1.7, Accelrys Software Inc., San Diego, CA, USA. 2006.
- [44] K.-H. Kim, D.H. Jung, D. Kim, A. Lee, K. Choi, Y. Kim, S.-H. Choi, Crystal structure prediction of organic materials: Tests on the 1,4-diketo-3,6-diphenylpyrrolo(3,4-c)pyrrole and 1,4-diketo-3,6-bis(4'-dipyridyl)-pyrrolo-[3,4-c)pyrrole, Dyes and Pigments, 89 (2011) 37-43.
- [45] A.D. Mighell, H.M. Ondik, B.B. Molino, Crystal data space-group tables, Journal of Physical and Chemical Reference Data, 6 (1977) 675-830.
- [46] H.R. Karfunkel, R.J. Gdanitz, Ab Initio prediction of possible crystal structures for general organic molecules, Journal of Computational Chemistry, 13 (1992) 1171-1183.
- [47] Z. Zhang, W. Hu, J. Cui, R. He, W. Shen, M. Li, Theoretical insights into the effect of a conjugated core on the hole transport properties of hole-transporting materials for perovskite solar cells, Physical Chemistry Chemical Physics, 19 (2017) 24574-24582.
- [48] K. Rakstys, S. Paek, P. Gao, P. Gratia, T. Marszalek, G. Grancini, K.T. Cho, K. Genevicius, V. Jankauskas, W. Pisula, Molecular engineering of face-on oriented dopant-free hole transporting material for perovskite solar cells with 19% PCE, Journal of Materials Chemistry A, 5 (2017) 7811-7815.
- [49] J. Roncali, Synthetic principles for bandgap control in linear π -conjugated systems, Chemical reviews, 97 (1997) 173-206.
- [50] W.-J. Chi, Q.-S. Li, Z.-S. Li, Exploring the electrochemical properties of hole transport materials with spiro-cores for efficient perovskite solar cells from first-principles, Nanoscale, 8 (2016) 6146-6154.
- [51] W.-J. Chi, Q.-S. Li, Z.-S. Li, Effects of Molecular Configuration on Charge Diffusion Kinetics within Hole-Transporting Materials for Perovskites Solar Cells, The Journal of Physical Chemistry C, 119 (2015) 8584-8590.
- [52] Y. Hua, J. Zhang, B. Xu, P. Liu, M. Cheng, L. Kloo, E.M.J. Johansson, K. Sveinbjörnsson, K. Aitola, G. Boschloo, L. Sun, Facile synthesis of fluorene-based hole transport materials for highly efficient perovskite solar cells and solid-state dye-sensitized solar cells, Nano Energy, 26 (2016) 108-113.